Ceramics-Silikáty 64 (2), 180-189 (2020)
www.ceramics-silikaty.cz doi: 10.13168/cs.2020.0007

INVESTIGATION OF ELECTRIC AND THERMAL PROPERTIES OF ALKALI-ACTIVATED ALUMINOSILICATES WITH A CNT ADMIXTURE

#OLDRICH ZMESKAL*, LUCIE TRHLIKOVA*, JAN POSPISIL*, LUKAS FIALA**, PAVEL FLORIAN*

*Faculty of Chemistry, Brno University of Technology,
Purkyňova 118, 612 00 Brno, Czech Republic
**Department of Materials Engineering and Chemistry, Faculty of Civil Engineering, Czech Technical University in Prague,
Thákurova 7, 166 29 Praha 6, Czech Republic

#E-mail: zmeskal@fch.vut.cz

Submitted October 15, 2019; accepted December 9, 2019

Keywords: Alkali-activated aluminosilicates, Carbon nanotubes, electric and dielectric properties, Thermal properties

The paper is focused on measurements of electric and thermal properties of alkali-activated aluminosilicates (AAAs) with a carbon nanotube (CNT) admixture. Such composites, fabricated from blast-furnace slag, quartz sand, water glass as an alkali activator, a small amount of electrically conductive CNT admixture and water exhibit better electric and thermal properties than the reference material without the CNT. Such an enhancement opens new practical applications, such as designing snow-melting, de-icing or self-sensing systems that do not need any external sensors to detect the current condition of the building's materials. Moreover, the economic aspect is more favourable in the case of AAA than that of Portland cement-based materials. The DC (direct current) electric properties are determined experimentally from the current-voltage (I-V) characteristics, the dielectric properties by means of impedance spectroscopy. Dielectric measurements allow us to determine the contribution of the individual components to the conductivity of the composite. The electric and thermal conductivities in the transverse direction were 16.16 μS·m^{-1} and 0.907 W·m^{-1}·K^{-1} for 0 % of CNT and 34.46 μS·m^{-1} and 1.298 W·m^{-1}·K^{-1} for 0.4 % of CNT, respectively.

INTRODUCTION

Presently, composites based on a cement matrix with electrically conductive admixtures are used in various applications, for example: self-sensing elements [1], self-heating or de-icing systems [1] or electromagnetic shielding systems [2]. Various forms of carbon particles, such as carbon black (CB), graphite powder (GP), carbon fibres (CFs) or carbon nanotubes (CNTs) are commonly used admixtures for enhancing the electric properties [3]. The electrically enhanced cement-based materials were studied due to their widespread use in the construction industry [4]. However, alkali-activated aluminosilicates (AAAs) with comparable strength, good chemical resistance and lower price were also investigated in terms of the mechanical, water transport and thermal properties [4, 6].

In this regard, the aim of the present work is to study the influence of the CNT admixture amount on the electric and thermal properties of the AAA composites (the thermal properties of AAAs have been reviewed [4, 7]). Specifically, the material includes three basic components: quartz sand as a filler, blast-furnace slag activated by water glass and a small amount of CNT.

The electric parameters of the AAA components are known from literature [8, 9]. However, the properties of the composite material involving such components can differ significantly. The electric and thermal properties of silicon oxide (sand) are summarised in the monography [8] and studied in the paper [9]. The presented results of the electric conductivity and the relative permittivity are about 0.10 S·m^{-1} and about 20 at 1 GHz and with a 20 % water concentration. The thermal conductivity for the sand depends on the porosity of the materials and is 2.7 - 2.8 W·m^{-1}·K^{-1} with porosity of 0.4. The dielectric properties of the aluminosilicates were studied in [9]. The results of the impedance analysis of the Portland cement paste obtained in the frequency region from 100 kHz to 15 MHz are summarised in the paper [9]. Two processes were recognised, one related to the solid matrix and the other to the liquid phase filling the pores. From the measurement presented in [10], a significant impact on the composition of the dielectric properties is evident. The spectra show one polar dielectric peak contained only alkali-activated slag, sand, water glass and water at low frequencies of the sample. This peek is shifted by the addition of a carbon admixture to the lower frequencies.

The specific heat of the slag in the wide interval of temperatures is presented in [12]. It varies from 700 J·kg^{-1}·K^{-1} at room temperature to 1100 J·kg^{-1}·K^{-1} at 600 °C. The presented thermal conductivities depend on the type of the alkali element (Li, Na, K) and differ in the interval (0.1 - 0.6) W·m^{-1}·K^{-1}.

Table 1. The composition of the used slag.

Component	SiO_2	Fe_2O_3	Al_2O_3	CaO	MgO	SO_3	Na_2O	K_2O	MnO	Cl
Amount [%]	39.66	0.47	6.45	40.12	9.50	0.72	0.33	0.55	0.65	0.05

MATERIALS AND SAMPLES

The set of AAA samples with different concentrations of the CNT admixture was prepared together with the reference AAA sample. All the studied materials (i.e., the reference AAA sample and the AAA samples with the different concentrations of the CNT admixture) were prepared from slag SMŠ 380 produced in Kotouč Štramberk s.r.o, from water glass SUSIL MP 2.0 (an alkali-activator), from water and from a different amount of multi-walled CNT Graphistrength CW 2-45 in mixture with carboxymethylcellulose (a homogenised 1 % CNT suspension). The samples of dimensions equal to 30 × 30 × 10 mm^3 were prepared by using normalised PG1 quartz sand, which fulfils the function (in this mixture) of the filler. The fabricated samples were immersed in water for the next 28 days. The compositions of the used slag is described in Table 1, the starting mixtures for these samples are described in Table 2.

Table 2. The composition of the fabricated AAA composites.

Component	CNT concentration (%)					
	0.00	0.05	0.10	0.2	0.30	0.40
slag (g)	140	140	140	140	140	140
sand (g)	140	140	140	140	140	140
water glass (g)	28	28	28	28	28	28
water (g)	57	57	57	57	57	57
CNT (mg)	0	70	140	280	420	560

The samples for the electric, dielectric and thermal measurements are presented in Figure 1a, b. The sample sizes (diameters and thicknesses) together with the basic parameters of the materials are described in Table 3. All the samples were contacted by the SPI Supplies conductive carbon paint, colloidal graphite in isopropanol. The measurements were realised in the transverse (about 10 mm in thickness) and longitudinal (about 30 mm in thickness) direction. The electric contact area was, in both cases, the same 10 × 30 mm^2. The arrangement of the experiment is demonstrated in Figure 1c.

The measurements of the current-voltage characteristics were carried out by using a Keithley 6517B electrometer and a Keithley 2410 source meter with integrated voltage sources. The frequency dependences were performed on a Solartron SI 1260 Impedance/Gain-Phase Analyzer with a Solartron Dielectric Interface 1296 device. The thermal measurements were carried out on the 30 × 30 mm^2 side of the samples in the transverse direction. The good thermal contact was ensured by a heat sink compound (Dow Corning 340). The arrangement of the temperature measurement apparatus is presented in Figure 1d.

Heating the samples were realised by an Agilent 6622A Power Supply and the temperatures were measured by an Agilent 34420A nanovoltmeter.

Table 3. The specifications of the studied samples.

	CNT conc. (%)	Mass (g)	Thickness (m)	Size/Diameter (m)	Volume (cm^3)	Bulk density ($kg \cdot m^{-3}$)
PMMA		3.53	0.0041	0.0303	2.98	1185
AAA-CNT composite	0.00	17.61	0.0105	0.0300	9.45	1863
	0.05	19.11	0.0110	0.0300	9.90	1930
	0.10	19.39	0.0110	0.0310	10.57	1834
	0.20	19.09	0.0110	0.0310	10.57	1805
	0.30	18.92	0.0115	0.0300	10.35	1828
	0.40	18.72	0.0110	0.0310	10.57	1770

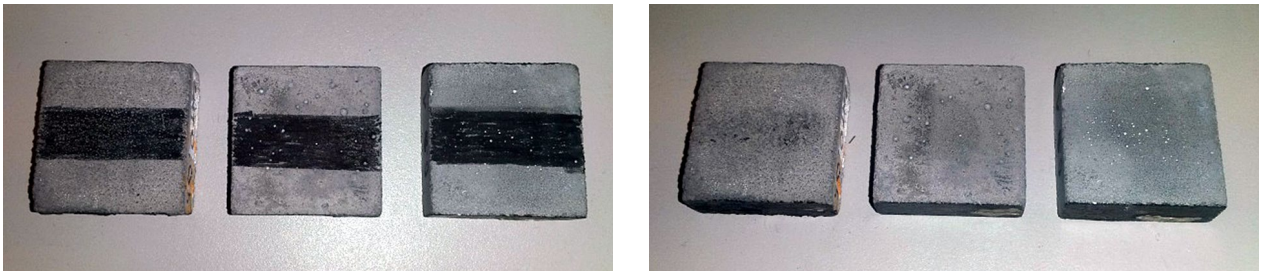

a) b)

Figure 1. The configuration of the measured samples for: a) the electric and dielectric measurements, b) the thermal measurements.

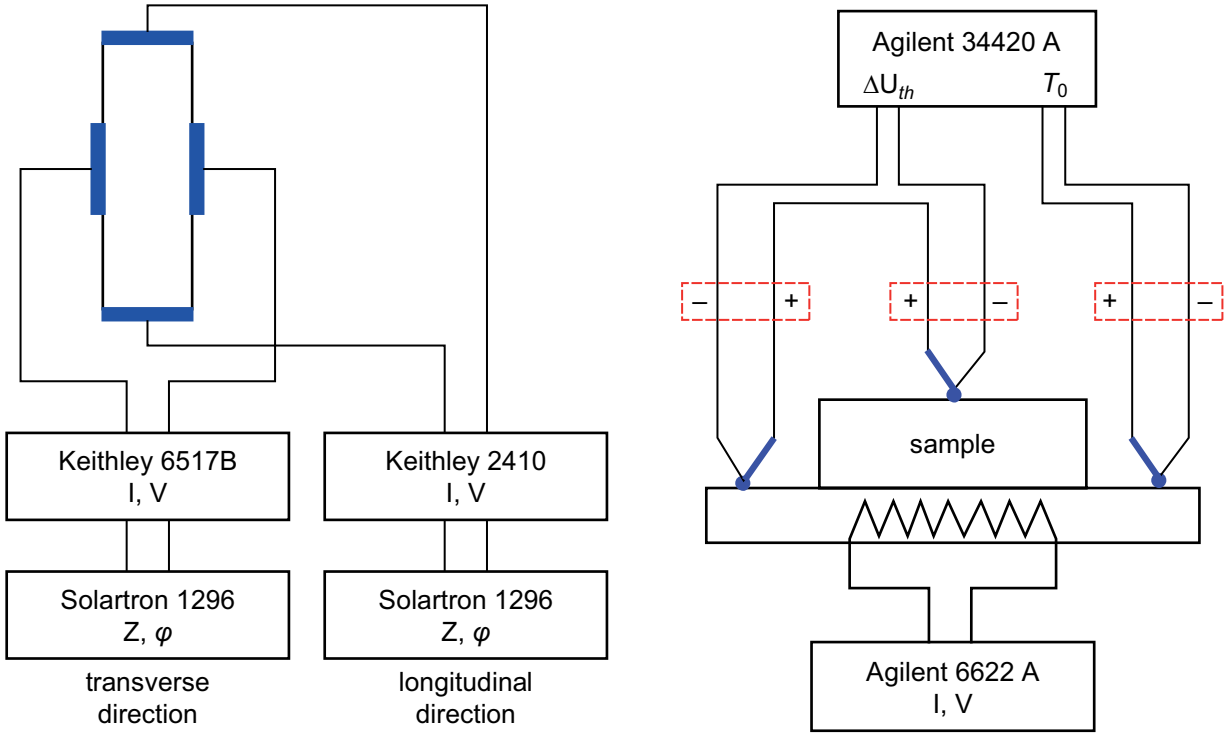

Figure 1. The measurement principle of: c) the current-voltage and impedance characteristics, d) the temperature transients.

ELECTRIC PROPERTIES

Experimental

The DC current-voltage characteristics were measured in the transverse direction by using a Keithley 6517B electrometer and in the longitudinal direction by a Keithley 2410 source meter. Embedded voltage sources of the equipment (± 1000 V) were used for sample power. This method of wiring devices allows one to measure the current-voltage characteristics in the transverse direction $I_T = f(V_T)$ for the different longitudinal voltages (V_L = const.), see Figure 1c. The current-voltage characteristics of the three types of samples are given in Figure 2. For better distinction of the I-V characteristics for the different longitudinal voltages V_L, the characteristics were shifted in the horizontal

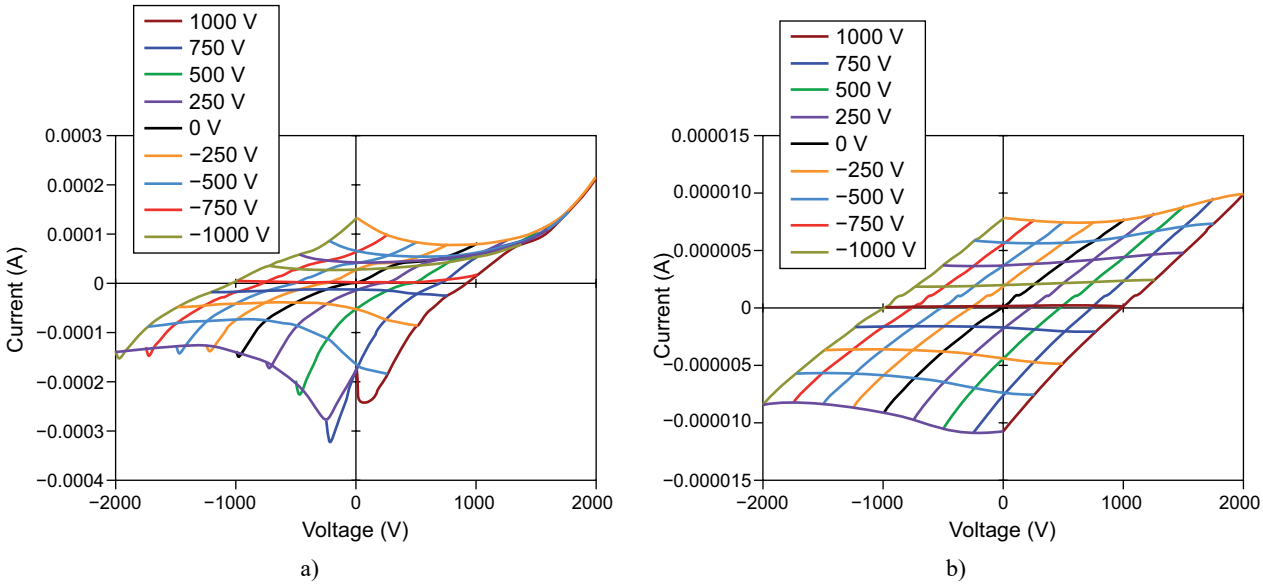

Figure 2. The dependence of the transverse current I_T on the sum of the transverse and the longitudinal voltages ($V_T + V_L$) of the selected samples for the different concentration of the CNT: a) 0.00 %, b) 0.10 %. The longitudinal voltage (V_L) is the parameter of dependence. *(Continue on next page)*

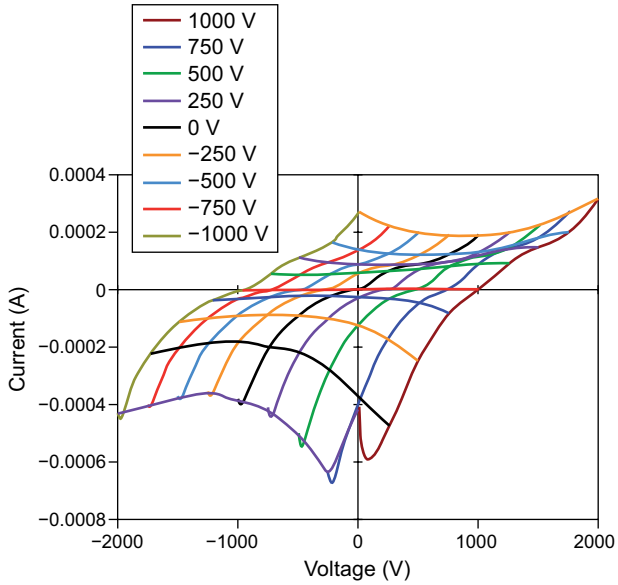

c)

Figure 2. The dependence of the transverse current I_T on the sum of the transverse and the longitudinal voltages ($V_T + V_L$) of the selected samples for the different concentration of the CNT: c) 0.30 %. The longitudinal voltage (V_L) is the parameter of dependence.

direction (the sum of the transverse and longitudinal voltages, $V_T + V_L$). It is evident that the current-voltage characteristics exhibit an ohmic (linear) character for a concentration of 0.10 % of the CNT (see Figure 2b) and the current is approximately one order less than for a smaller and larger concentration of the CNT (see Figures 2b, c). Moreover, for these cases, the characteristics have a nonlinear character.

Results

The transverse and the longitudinal DC electric conductivity of the studied samples are presented in Table 4, and in Figure 3, respectively. It is evident that the sample with 0.1 % of CNT exhibited the smallest electric conductivity, which agrees with the current-voltage characteristics presented in Figure 2. In the case of the 0.1 % CNT concentration, the dependences are linear, because the polarisation of the dipoles is compensated for. The nonlinear characteristics (for smaller and larger concentrations of the CNT) are caused by dipoles of the molecules of the alkali-activated slag and sand that are not compensated. The differences between the current-voltage characteristics for the different V_L are caused by the inhomogeneities of the samples (for the different V_L, there is a different perpendicular electric field and a different path of electric current). More detailed information can be obtained by using the Solartron SI 1260 impedance analyser.

The dependence of the electric conductivity (in the longitudinal and transverse direction) on the concentration of the CNT at zero voltage in a perpendicular direction (transverse, longitudinal) is presented in Figure 3.

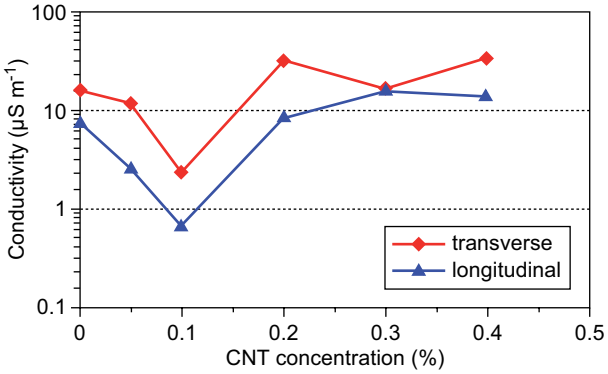

Figure 3. The dependence of the electric conductivity on the concentration of the CNT in the alkali-activated blast-furnace slag composite measured in the transverse and longitudinal direction.

DIELECTRIC PROPERTIES

Theory

The dielectric properties can be expressed by the impedance Z, which is described by the resistance R and the capacitive reactance X_C as follows

$$Z = R + jX_C = |Z| \exp(j\varphi), \qquad (1)$$

where $j = \sqrt{-1}$ is the imaginary unit, $|Z| = \sqrt{R^2 + X_C^2}$ is the impedance modulus and $\varphi = \text{arctg}(X_C/R)$ is the phase shift between the real and imaginary part.

Table 4. The specifications of the studied samples.

	CNT conc. (%)	Transverse direction		Longitudinal direction	
		resistance (MΩ)	conductivity (μS·m^{-1})	resistance (MΩ)	conductivity (μS·m^{-1})
AAA-CNT composite	0.00	2.17	16.16	12.25	7.77
	0.05	3.10	11.81	36.05	2.52
	0.10	14.46	2.37	136.37	0.67
	0.20	1.09	31.64	10.51	8.65
	0.30	2.25	17.00	5.47	15.91
	0.40	1.00	34.46	6.69	13.59

In these equations, $R = \rho^{*} \cdot l/S = l/(\sigma \cdot S)$ and $X_C = -1/(\omega \cdot C) = -l/(\omega \cdot \varepsilon \cdot S)$, where ρ^{*} is the electric resistivity, l is the thickness, S is the contact area, σ is the electric conductivity, ω is the angular frequency and ε is the electric permittivity. In the case of the dispersion of the electric charge carriers during transport through the material, the constant phase element (CPE), described by Equation 2, needs to be taken into consideration:

$$Z = \frac{1}{Y_0\,\omega^n}\,\exp\left(-\frac{j\pi}{2}\,n\right). \qquad (2)$$

The capacitance $X_C = -1/(\omega \cdot Y_0) = -1/(\omega \cdot C)$, (for $n = 1$), resistance $R = 1/Y_0 = 1/G$, (for $n = 0$) or inductance $X_L = \omega/Y_0 = \omega \cdot L$, (for $n = -1$) are special cases of this term. This means that the Y_0 parameter, therefore, depends on the type of components (resistor R, capacitor C, inductor L, or, generally, the constant phase element CPE).

Experimental section

Measurements of the AC (alternating current) characteristics were carried out (for the transverse and longitudinal direction of the samples) on a Solartron SI 1260 impedance analyser with a Solartron 1296 dielectric interface in the frequency range of 0.01 Hz to 1 MHz. The obtained results are presented in Figure 4. It is evident that the transverse impedance in low frequencies (see Figures 4a, c) is about one order of magnitude lower than for the longitudinal direction – the distance of the contacts in the transverse direction is approximately three times lower than in the longitudinal direction. The phase shift (see Figures 4b, d) is nearing the zero value for the low frequencies, which indicates the resistive character of the behaviour. The results are in a good agreement with the DC measurement results (see Table 4). From Figure 4b, d, it is also evident that the impedance phase shift (dependence on the frequency) is more complicated for the longitudinal than for the transverse arrangement of the contacts. It can be due to the inhomogeneity and anisotropy of the samples and due to the higher dispersion for the charge carriers over the longer distance. The electric properties of the com-posites (see Figure 1 and Table 2) and the charge transport can also be affected by the electric properties of each component, which can bind a dopant represented by the CNT conductive component.

Results

The dependence of the reactance X on the resistance R (Cole-Cole diagram, Figure 5a) and the dependence of the serial capacity C on the serial resistance R (or conductance, see Figure 5b) were calculated using the formulas outlined in the theoretical part. The differences

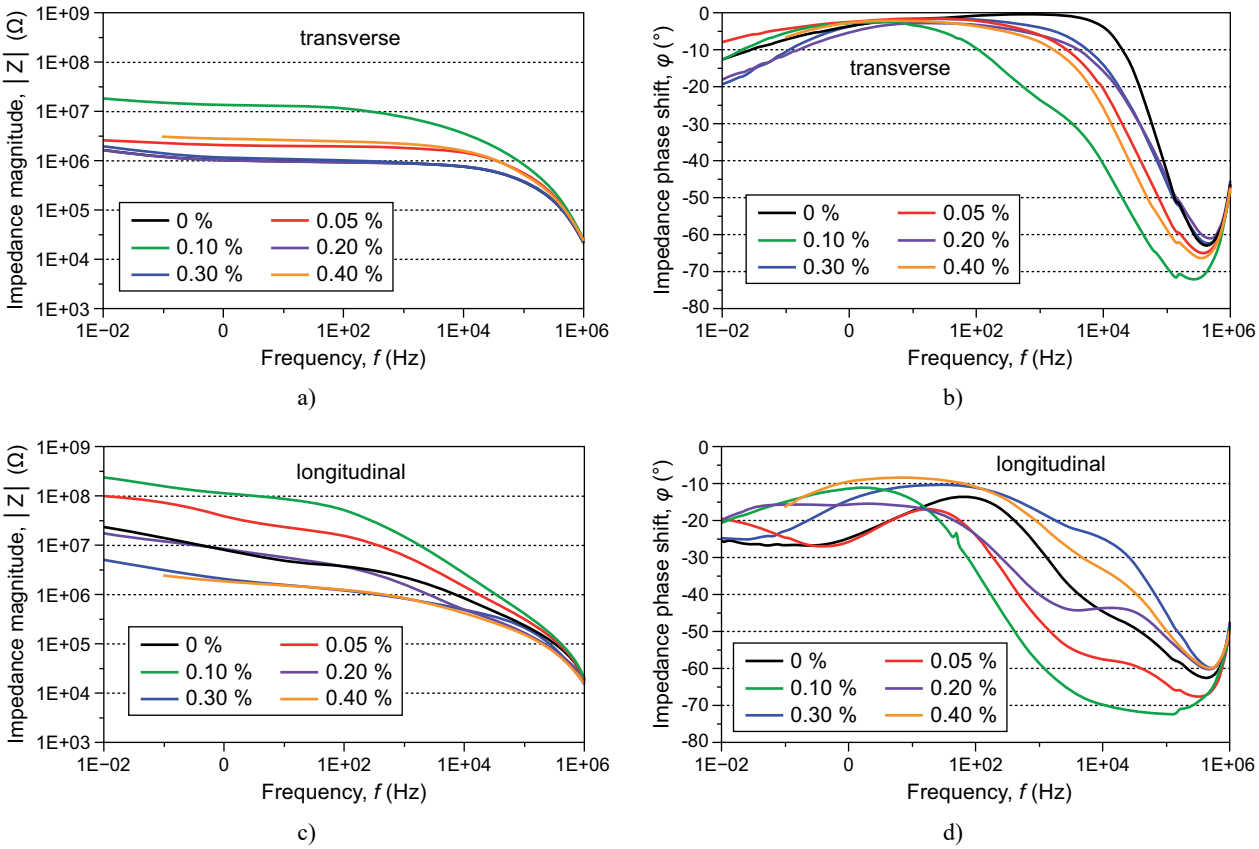

Figure 4. The impedance characteristics: dependence of the impedance magnitude (a, c) and the phase shift (b, d) on the frequency for the longitudinal (a, b) and the transverse (c, d) directions.

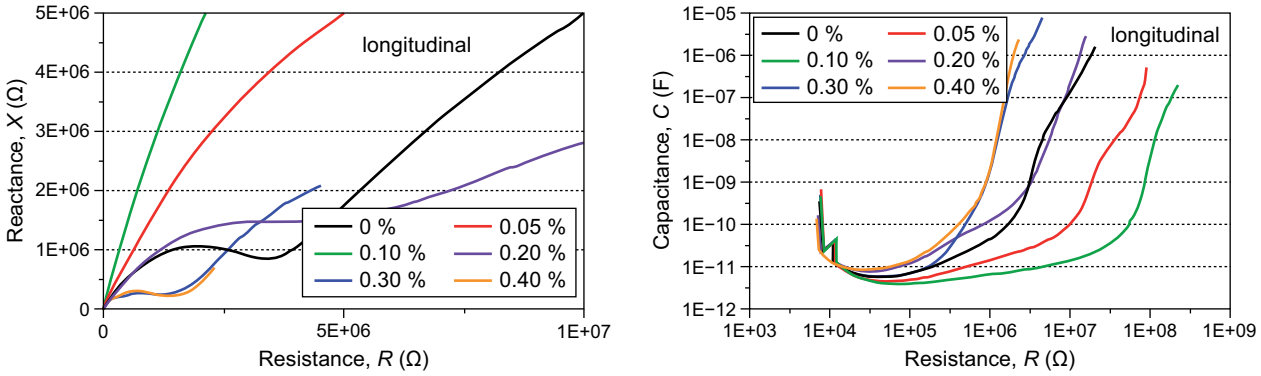

Figure 5. The dependence of: a) the reactance X on the resistance R (i.e., Cole-Cole diagram) and b) the capacitance C on the resistance R.

between the responses of the samples with the different CNT concentrations are obvious. The detailed analysis showed that a predicted equivalent circuit consists of parallel resistors and a capacitive CPE corresponding to the individual components (quartz sand, alkali-activated slag – aluminosilicate, pore solution and CNT) connected in series (see the scheme in Table 5).

The electric parameters of the components (resistance, capacitance and diffusion CPE parameter) for the longitudinal direction are summarised in Table 5. The calculated values relativized to the sample size are then given in Figure 6.

The results presented in Figure 6 revealed that higher CNT concentrations lead to an increase the

Table 5. The specifications of the studied samples.

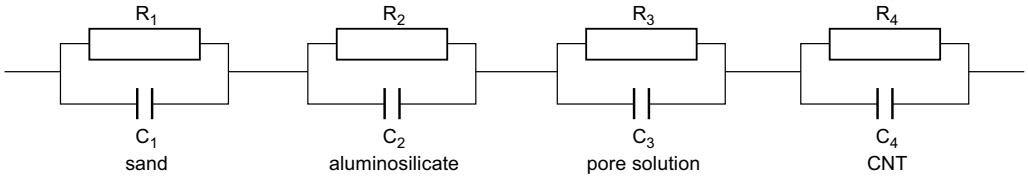

Longitudinal direction	R_1 (MΩ)	C_1 (nF)	n_{C1}	R_2 (MΩ)	n_{R2}	C_2 (nF)	R_3 (MΩ)	C_3 (nF)	n_{C3}	R_4 (MΩ)	C_4 (nF)	n_{C4}
0.00 %	8	200	0.66	7.0	0.38	3.0	3.4	0.7	0.67	0.10	0.020	1.00
0.05 %	45	30	0.70	25.0	0.33	6.0	20.0	0.4	0.68	0.10	0.050	1.00
0.10 %	18	0.2	0.75	4.5	0.20	10.0	2.0	0.8	0.84	6.00	0.019	1.00
0.20 %	5	70	0.64	3.5	0.42	7.0	5.0	1.8	0.65	0.13	0.018	0.98
0.30 %	3	2000	0.60	1.6	0.35	0.9	0.9	2.5	0.65	0.35	0.015	0.91
0.40 %	3	7000	1.00	1.2	0.21	0.1	0.8	1.8	0.70	0.20	0.040	0.90

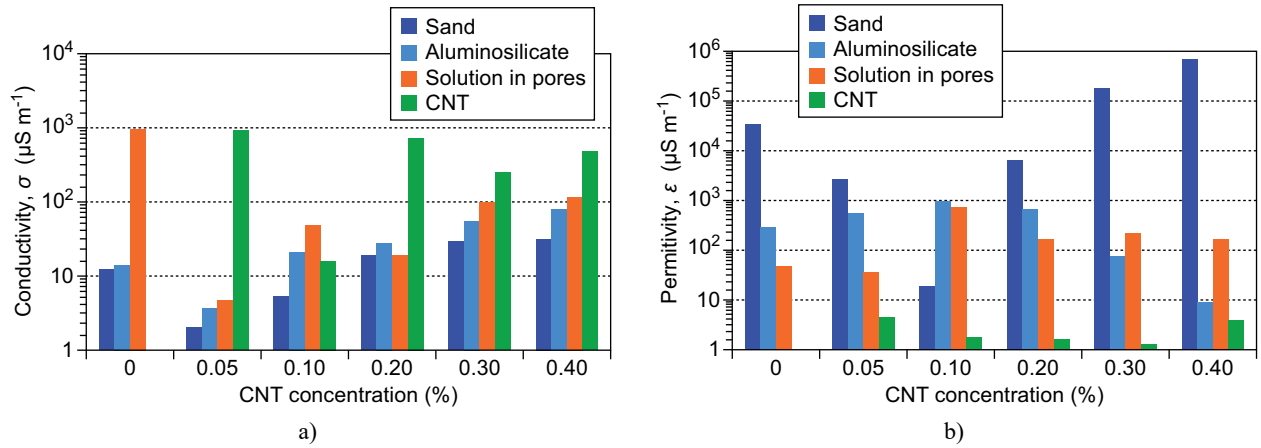

Figure 6. The electric (a), dielectric (b) and CPE (c) parameters in the longitudinal measurements. *(Continue on next page)*

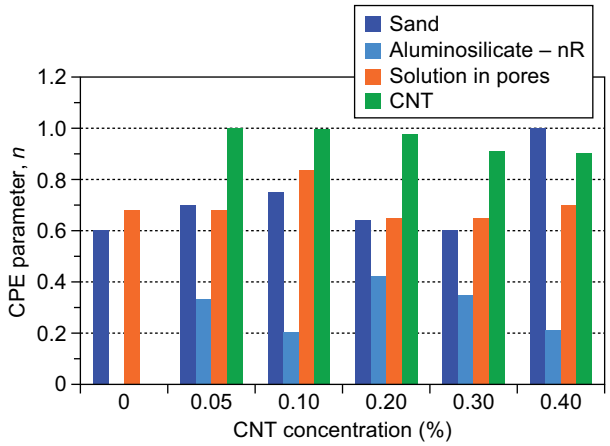

c)

Figure 6. The CPE (c) parameters in the longitudinal measurements.

electric conductivity of the composite significantly more than the other components. The capacity is, in the case of the CNT, of several orders of magnitude lower (in comparison with other components) and has almost with no dispersion, (the CPE parameter is approximately equal to one). On the other hand, the electric conductivity of the sand (which is in the same amount as the alkali-activated slag) is very small – conversely, the capacity (the effective permittivity) is several orders of magnitude higher. It is also caused by the dispersion in the AC field (the CPE parameter of capacity is about 0.6). The alkali-activated slag has higher electric conductivity than the sand and several orders of magnitude lower electric capacity – the dispersive nature of the free electric charge contributes to the electric conductivity (the value of its diffuse (CPE) parameter varies from 0.2 to 0.42 depending on the CNT concentration, see Figure 6c). The last component is a pore solution – its conductivity and permittivity (dielectric constant) is comparable to the alkali-activated blast furnace slag, and its CPE parameter n is comparable to sand.

THERMAL PROPERTIES

Theory

The thermal properties of the materials were calculated using the Carslaw Jaeger mathematical model [14, 15]. The temperature response of the heating is described as follows:

$$\Delta T(t) = At^{\alpha}\exp\left(-\frac{h^2}{4at}-\frac{4at}{R^2}\right), \text{ resp.}$$

$$\Delta T(t) = \Delta T_0 (t/t_{\mathrm{D}})^{\alpha}\exp\left[-\left(\frac{t_{\mathrm{D}}}{t}+\frac{t}{t_{\mathrm{R}}}\right)\right], \qquad (3)$$

where A is the coefficient of the thermal absorption, h is the distance of the thermal sensor and the heat source, a is the thermal diffusivity, R is the heat loss parameter (must be higher than the heat source diameter), $\Delta T_0 = At_{\mathrm{D}}^{\alpha}$ is the temperature difference in a steady state, $t_D = h^2/4a$ is the diffusion time, $t_R = R^2/4a$ is the relaxation time. The ratio of the relaxation and the diffusion time $t_R/t_D = R^2/h^2$ determines the influence of the measured thermal responses by the heat losses.

The heat source is characterised by the value of $\alpha = \alpha_0 + (D - E)/2$, where E is a dimension of the space for spreading the heat (for volume it is $E = 3$). D is the space dimension of the heating ($D = 0, 1, 2, 3$ sequentially for a point, linear, planar and volume heating, respectively), and α_0 defines the type of heating ($\alpha_0 = 0, 1, 2$ sequentially for pulse, step-wise and ramp-wise heating, respectively) [16, 17].

The thermal diffusivity a, the thermal conductivity λ and the specific heat capacity c_{p} can be then determined as

$$a = \frac{\mathrm{d}\ln\Delta T}{\mathrm{d}t}h^2 = \frac{h^2}{4t_{\mathrm{D}}},\ \lambda = \Lambda\frac{h}{S} = \frac{P}{\Delta T}\frac{h}{S},\ c_{\mathrm{p}} = \frac{P}{m}\frac{\mathrm{d}t}{\mathrm{d}T} = \frac{\lambda}{\rho a}, \qquad (4)$$

where P is the heat power, S is the surface area, ρ is the bulk density of material, and $m = \rho \cdot h \cdot S$ is the mass of the measured sample.

Experimental section

The thermal properties were measured in a Dewar bottle [18], where heat was supplied to the system through a built-in resistor in the planar metal source (settings: the power of the pulse generated by the Agilent 6622A Power Supply was 4.18 W; the measurement duration was 12 hours). K-type thermocouples were used for the measurement of the temperature difference between the hot and cold surface ($\mathrm{D}T_{\mathrm{c}}$) of the sample as the thermoelectric voltage $\mathrm{D}U_{\mathrm{th}}$ using an Agilent 34420A nanovoltmeter (Channel 1) and another included K-type thermocouple was used to obtain the temperature of the heat source T_0 (Agilent 34420A nanovoltmeter, channel 2), see Figure 1d. In this case, the following applies: $\mathrm{D}T_{\mathrm{c}} = T_0 - T_1$, where T_1 was calculated from the temperature T_0 and the thermoelectric voltage $\mathrm{D}U_{\mathrm{th}}$ (using a calibration curve of a K-type thermocouple). The thermal measurements that were carried out for all the samples with the different CNT concentrations in the transverse direction are then presented in Figure 7a.

It is evident (see Figure 7a) that the highest change in the temperature was observed for the sample with a concentration of 0.40 mass. % CNT. It indicates the lowest thermal conductivity of this sample.

The specific heat capacity can be estimated from the slope of the transient response. The sample with 0.30 % concentration of the CNT had the highest specific heat capacity (the fastest response of the temperature to the heating pulse), while the reference sample and the sample with 0.05 % CNT had the smallest.

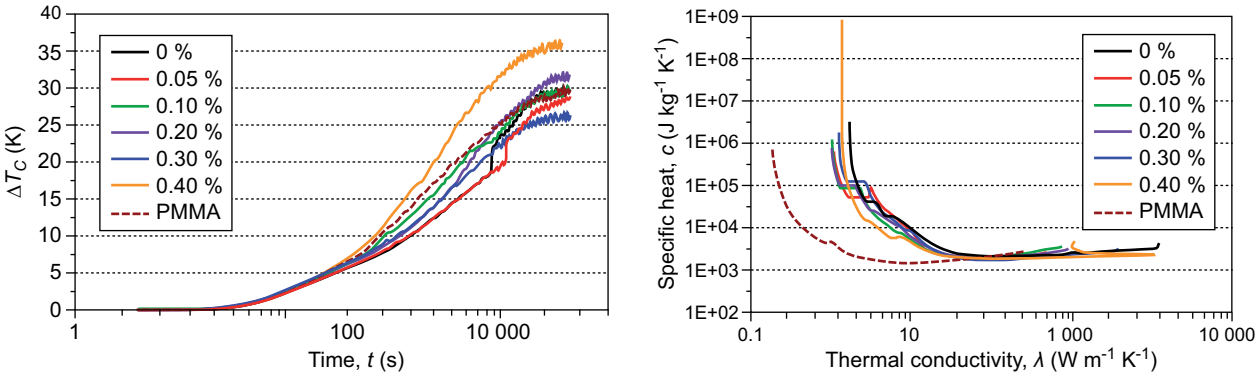

a) b)

Figure 7. a) The responses of the temperature changes between the hot and cold surface of the sample (T0 – T1) on the time for the transverse direction of the measurement; b) The dependence of the specific heat capacity on the thermal conductivity of the AAA samples with the CNT admixtures calculated for the determination of the real values of the specific heat and thermal conductivity by the differential method.

The PMMA (polymethylmethacrylate) sample had a temperature response comparable to the responses of the AAA-CNT samples and, therefore, their thermal parameters are comparable.

Results

The evaluation of the experimental data was carried out analogously to those presented in the previous chapter (see Chapter 4.: Dielectric properties). Firstly, the difference of the temperature limit between the hot and cold side of the sample was determined and using the relationships presented in the theoretical part of this chapter – the dependencies of the specific heat capacity on the thermal conductivity were calculated. The results are given in Figure 7b. The vertical tangents in these dependencies determine the thermal conductivity of the samples (in the steady state), the horizontal tangents determine the specific heat (for short times, the greatest slope of the transient response). Deviations of the specific heat from the horizontal tangent for the short times are related to the dispersive nature of the heat transfer.

The summary of the results obtained by fitting the mathematical model is given in Table 5. It is evident that the highest value of the specific heat capacity and the minimum value of the thermal conductivity is for the reference sample. The results for all the samples can be compared with a set of values for a polymethylmethacrylate (PMMA) material with known thermal properties (the table value of the thermal conductivity is about 0.17 $W \cdot m^{-1} \cdot K^{-1}$, the specific heat is about 1400 $J \cdot kg^{-1} \cdot K^{-1}$). The selected results from Table 6 are presented in bar graphs (see Figure 8). The results agreed with the conclusions made in the previous section (see Chapter Dielectric properties).

CONCLUSIONS

The Alkali-activated aluminosilicates are promising materials for their use in heating and sensing systems due their electric, dielectric and thermal properties.

The distribution of the DC electric conductivity in the samples was determined from the current-voltage characteristics in the transverse and longitudinal direction. It was observed that, in both directions, the sample with 0.10 % CNT concentration exhibited a minimal electric conductivity (transverse direction: 2.37 $\mu S \cdot m^{-1}$, longitudinal direction: 0.67 $\mu S \cdot m^{-1}$, respectively). The electric conductivity of the rest of the samples was more than 10 times higher. Therefore, the materials with a higher concentration of CNT are better for self-heating systems.

Table 3. The thermal properties of the studied composites.

CNT concentration	P (W)	ρ ($kg \cdot m^{-3}$)	ΔT_c (K)	t_D (s)	a ($mm^2 \cdot s^{-1}$)	c ($J \cdot kg^{-1} \cdot K^{-1}$)	λ ($W \cdot m^{-1} \cdot K^{-1}$)
PMMA	0.92	1 186	30.25	62	0.108	1 444	0.185
0.00 %	4.18	1 871	30.24	64	0.410	2 101	0.907
0.05 %	4.18	1 930	29.26	52	0.538	1 681	0.982
0.10 %	4.18	1 834	30.03	65	0.444	1 955	0.957
0.20 %	4.18	1 806	32.20	65	0.436	1 887	0.939
0.30 %	4.18	1 828	26.78	48	0.658	1 658	1.180
0.40 %	4.18	1 771	36.87	71	0.410	1 788	1.298

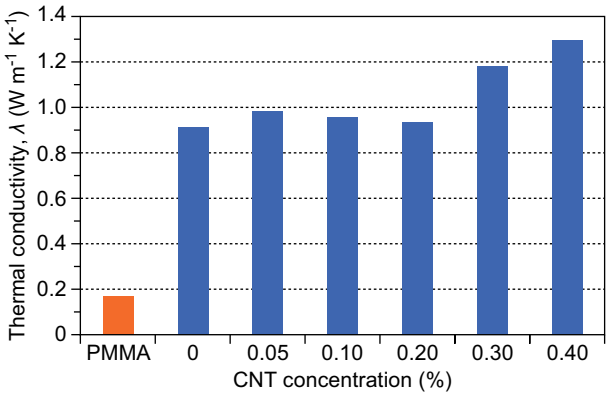

a)

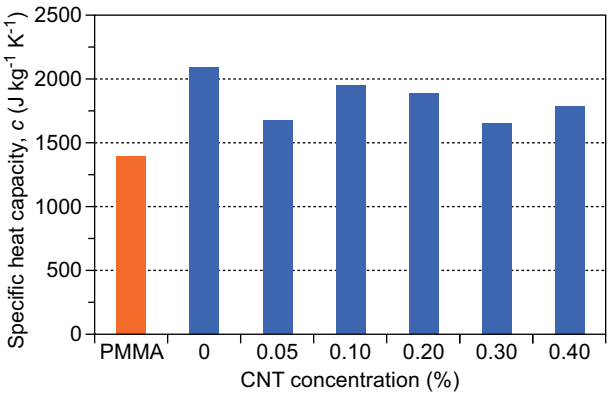

b)

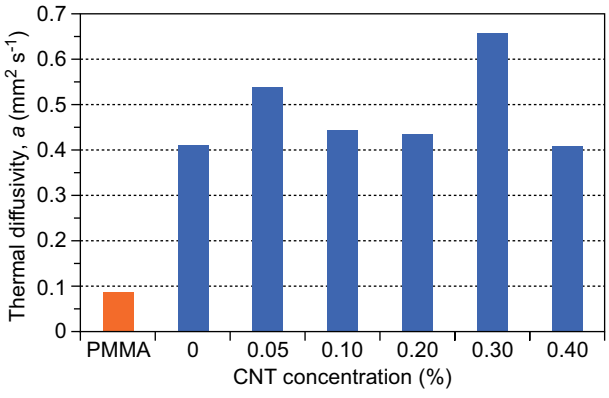

c)

Figure 8. The thermal parameters of the samples for the transverse measurement: a) thermal conductivity, b) specific heat and c) thermal diffusivity.

The AC conductivity of the samples in the transverse and longitudinal directions confirmed the results of the DC measurements. Besides, the results of the AC measurements were used for the evaluation of the RC values of the elements represented by the alkali-activated blast-furnace slag, quartz sand, CNT and pore solution in the pores. The measurements showed that the dispersion in the longitudinal direction is larger (the impedance spectrum is more complicated) than in the transverse direction.

The material with the lowest electric conductivity (the sample with a 0.10 % CNT concentration) exhibited the local maximum in the specific heat capacity dependence on the concentration of the CNT (1955 $J \cdot kg^{-1} \cdot K^{-1}$). The sample with 0.40 % CNT concentration has the highest value of the thermal conductivity and the lowest thermal diffusivity. The results were compared with the PMMA measurements (λ = 0.165 $W \cdot m^{-1} \cdot K^{-1}$, c = 1 394 $J \cdot kg^{-1} \cdot K^{-1}$), which is in good agreement with the tabulated values. The temperature measurements confirmed the correlation between the thermal, electric and dielectric properties.

The sample with 0.1 % of CNT had the minimal electric conductivity due to its low ionic conductivity. It is explained by an increase in the crystallinity of the activated slag by the CNT. For higher CNT concentrations, this effect not visible due to the agglomeration of the CNT.

The electrical properties of the AAA materials depend on the presence of the ionic species in the matrix which is related to the degree of the alkali activated reaction. This method could help to determine the conversion degree, heat evolution, development of compressive strength, etc.

Acknowledgements

The authors would like to thank the Ministry of Education, Youth and Sports of the Czech Republic for its support by the Czech Science Foundation, under Project No. 19-11516S and for support by project FCH-S-19-5834.

REFERENCES

1. Wen S., Chung D.D.L. (2007): Electrical-resistance-based damage self-sensing in carbon fiber reinforced cement, *Carbon*, *45*, 710–716. doi: 10.1016/j.carbon.2006.11.029
2. Won J.P., Kim, Lee S.J., Lee J.H., Kim R.W. (2014): Thermal characteristics of a conductive cement-based composite for a snow-melting heated pavement system. *Composite Structures*, *118*, 106–111. doi: 10.1016/j.compstruct.2014.07.021
3. Guan H., Liu Y., Duan C.K., Cheng J. (2006): Cement based electromagnetic shielding and absorbing building materials *Cement and Concrete Composites*, *28*, 468–474. doi: 10.1016/j.cemconcomp.2005.12.004
4. Zuda L., Cerny R. (2009): Measurement of linear thermal expansion coefficient of alkali-activated aluminosilicate composites up to 1000 °C. *Cement and Concrete Composites*, *31*, 263-267. doi: 10.1016/j.cemconcomp.2009.02.002
5. Sedaghat A., Ram M.S.K., Zayed1 A., Kamal R., Shanahan N. (2014): Investigation of Physical Properties of Graphene-Cement Composite for Structural Applications. *Open Journal of Composite Materials*, *4*, 12–21. doi: 10.4236/ojcm.2014.41002
6. Zuda L., Drchalova J., Rovnanik P., Bayer P., Kersner Z., Cerny R. (2010): Alkali-activated aluminosilicate com-

posite with heat-resistant lightweight aggregates exposed to high temperatures: mechanical and water transport properties. *Cement and Concrete Composites*, *32*, 157–163. doi: 10.1016/j.cemconcomp.2009.11.009

7. Zuda L., Pavlik Z., Rovnanikova P., Bayer P., and Cerny R. (2006): Properties of Alkali Activated Aluminosilicate Material after Thermal Load. *International Journal of Thermophysics*, *27*, 1250–1263. doi: 10.1007/s10765-006-0077-7
8. Bansal N.P., Doremus R.H. (1986). *Handbook of Glass Properties*. Academy Press, Inc.
9. Santamarina J.C., Ruppel C. /2008). The Impact of Hydrate Saturation on the Mechanical, Electrical, and Thermal Properties of Hydrate-Bearing Sand, Silts, and Clay. in: *Proceedings of the 6th International Conference on Gas Hydrates*, Vancouver, Canada, pp. 1 – 2. doi: 10.1190/1.9781560802197.ch26
10. Cabeza M., Merino P., Miranda A., Novoa X.R., Sanchez I. (2002): Impedance spectroscopy study of hardened Portland cement paste *Cement and Concrete Research*, *32***,** 881–891. doi: 10.1016/S0008-8846(02)00720-2
11. Lunak M., Kusak I., Chobola Z. (2016): Carbon Admixtures Influence on the Electrical Properties of Slag Mortars Focusing on Alternating Conductivity and Permittivity. *Procedia Engineering*, *151***,** 236–240. doi: 10.1016/j.proeng.2016.07.359
12. Mills K. (2011): The Estimation of Slag Properties. *Southern African Pyrometallurgy*.
13. Carslaw H.S., Jaeger J.C. (1986): *Conduction of Heat in Solids*, 2nd ed., Oxford University press.
14. Zmeskal O., Vala M., Weiter M., Stefkova P. (2009): Fractal – Cantorian geometry of space-time. *Chaos, Solitons & Fractals*, *42*, 1878–1892. doi: 10.1016/j.chaos.2009.03.106
15. Zmeskal O., Stefkova P., Dohnalova L., Barinka R. (2012): Use of PCM Boards for Solar Cell Cooling. *International Journal of Thermophysics*, *34*, 926–938. doi: 10.1007/s10765-012-1196-y
16. Trhlikova L., Zmeskal O., Prikryl R., and Florian P. (2015): Thermal Properties of Mannitol Derivative. *Advanced Materials Research*, *851***,** 181–186. doi: 10.4028/www.scientific.net/AMR.1126.181
17. Zmeskal O., Trhlikova L. and Dohnalova L. (2016): Thermal properties of an erythritol derivative. *AIP Conference Proceedings*, *1738***,** 280008. doi: 10.1063/1.4952068
18. Trhlikova L., Zmeskal O., Psencik P., Florian P. (2016): Study of the thermal properties of filaments for 3D printing. *AIP Conference proceedings*, *1752***,** 040027. doi: 10.1063/1.4955258
19. Trhlikova L., Prikryl R. and Zmeskal O. (2015): Study of thermal properties of insulating materials. *AIP Conference Proceedings*, *1648***,** 410012. doi: 10.1063/1.4912641